

A COMPARISON OF FALSE COLOR COMPOSITES IN MAPPING
AND DISCRIMINATING BETWEEN SALT-AFFECTED SOILS
IN KINGS COUNTY, CALIFORNIA

By

Carmelita Gutierrez

A RESEARCH PAPER

submitted to

THE GEOSCIENCES DEPARTMENT
OREGON STATE UNIVERSITY

in partial fulfillment of the requirements for the degree of

MASTER OF SCIENCE

GEOGRAPHY PROGRAM

June 2002

Directed by
Dr. Charles L. Rosenfeld

In loving memory, I dedicate this work to my grandmother,
Carmen Estrada
luz de mis ojos

ACKNOWLEDGEMENTS

I would like to thank Dr. Charles Rosenfeld for his guidance, encouragement, and unwavering optimism throughout the design and writing of this paper. I would also like to thank Dr. Matzke for his constant, invaluable support and advice, especially in challenging times. My sincerest gratitude for Dr. Kimerling, who provided much-needed technical advice, encouragement, and good cheer.

Several components of this paper would have never been possible without the support of Kerry Arroues, soil scientist with USDA-NRCS in Kings County. I am grateful for the invaluable information, materials, and contacts Mr. Arroues provided, which provided the crucial understanding of soil conditions and land use practices in Kings County.

Special thanks also go to Sandee Lovelady, soils technician at OSU's Central Analytical Lab, who analyzed the soil samples for this study, and went beyond her call of duty to complete the typically time-consuming laboratory analyses so I could continue with my research.

This acknowledgment would not be complete without recalling, with gratitude, my undergraduate professors, Drs. Ron Taskey and Thomas Ruehr, whose rigorous demands and high standards in research design and writing facilitated the completion of this research paper; and, of course, for Dr. Preston, the first to instill in me the passion for geography and the seed for undertaking this research project.

Warmest thanks go to Joanne Van Geest and Melinda Peterson for their help throughout my graduate career, especially toward the end, when they provided so much administrative help. I am fortunate to have had your help.

I would also like to thank my family, especially my parents: my mom for her love, encouragement, inspiration, and unofficial sponsorship of my research; and my father for his love, unwavering belief in me, and genuine interest in my research. Gracias.

Last, but never least, I'd like to thank my husband, Bernie, for his good thoughts and calming energy and for bearing the brunt of having to live with a graduate student struggling through the research process.

TABLE OF CONTENTS

ACKNOWLEDGMENTS.....	ii
TABLE OF CONTENTS	iii
LIST OF FIGURES.....	iv
LIST OF TABLES	v
ABSTRACT.....	1
INTRODUCTION.....	1
MATERIALS AND METHODS	4
Study area.....	4
Image acquisition and pre-processing.....	7
Field sampling and soil analysis.....	8
Classification of Landsat TM data	12
Comparison of false color composites	13
RESULTS AND DISCUSSION	15
Preliminary comparison of false color composites	15
Interpretation of spectral profiles	18
Comparison of classified images.....	21
CONCLUSIONS and RECOMMENDATIONS	30
REFERENCES	35
APPENDIX	38

LIST OF FIGURES

Figure

1.	Location of study area within Kings County, California	5
2.	Location of field sample points mapped on a false color composite (FCC) image using Landsat TM bands 4, 3, and 2.	9
3.	Color composites of Landsat Thematic Mapper data for the study area.....	17
4.	Spectral profiles of salt-affected and nonsaline soils.	18
5.	Spectral profiles of salt-affected soils along the first three principal components of the Tasseled Cap transformation.	18
6.	Spectral profiles of salt-affected and sandy soils from soil samples west of Blakely Canal.	19
7.	Total area per class for each false color composite.....	21
8.	Maximum likelihood classification algorithm applied to training data from the Landsat TM image.....	23
9.	Transformed divergence values between sandy soil signatures and salt-affected soil signatures.	25
10.	Transformed divergence values between salt-affected signatures.	27
11.	Salt-affected soil signatures plotted on the feature space of several bands for each false color composite.	29

A COMPARISON OF FALSE COLOR COMPOSITES IN MAPPING AND DISCRIMINATING BETWEEN SALT-AFFECTED SOILS IN KINGS COUNTY, CALIFORNIA

ABSTRACT: Spectral profiles, transformed divergence values, and feature space derived from Landsat Thematic Mapper (TM) data were used to analyze the ability of four false color composites to discriminate between different classes of salt-affected soils. To compare the spatial distribution of salt-affected soil classes, maps were generated for each false color composite using the maximum likelihood classification algorithm applied to training data from the Landsat TM image. Soil samples were collected and analyzed to correlate brightness values from Landsat data with surface soil characteristics. Few differences occurred in the number of pixels assigned to each class among the four false color composites. Based on signature separability data, no false color composite provided an overall improvement in discriminating between salt-affected soil classes. Poor separability occurred in the western portion of the study area between several classes: saline and saline-sodic; sandy soils and saline soils; sandy soils and saline-sodic soils; and between nonsaline and sodic soils. Greater separability between classes occurred in the eastern portion of the study area. The low discrimination between several soil types and salt-affected soils using remote sensing data illustrates the challenges in mapping salt-affected soils.

INTRODUCTION

Satellite remote sensing is widely used in assessing and monitoring soil degradation. Satellite images of sand drifts and dune movements are used to assess desertification; and soil erosion is monitored by measuring river sedimentation detected on satellite images (Mishra 1994; Kaushalya 1992; Barrett and Hamilton 1986; Kumar et al. 1993). Salinization, the accumulation of soluble salts in soils, is one form of soil degradation extensively studied using remotely sensed data.

Salt accumulation in soils is a major threat to the sustainability of agricultural lands worldwide. Since 1985, thousands of acres of California's agricultural land have been retired

due to the high concentrations of salts in the topsoil and subsoil (Arroues 2001, personal communication). In an attempt to decrease salinization on agricultural lands, scientists are developing methods for detecting and proper monitoring of salt-affected soils. Within the last twenty years, satellite remote sensing information has been used to monitor agricultural lands at risk due to salinization. The temporal and spatial scales of satellite remote sensing data can facilitate seasonal and yearly monitoring of agricultural lands encompassing large areas (Dwivedi and Sreenivas 1998; Dwivedi et al. 1999; Rao and Venkataratnam 1991; Sujatha et al. 2000). In addition, satellite image information can supplement field data when mapping soil surface conditions and spatial variations of degraded soils. (Evans et al. 1995; Kalra and Joshi 1996; Peng 1998; Sharma and Bhargava 1988).

Different surface features associated with soil degradation have relatively distinct spectral characteristics, which allow for the application of digital image processing in detecting soil surface variations. Research on the spectral characteristics of salt-affected soils reveals high reflectance values in comparison to other soil surface features, enabling the use of satellite imagery to detect these soil characteristics (Satterwhite and Henley 1987). In the visible portion of the electromagnetic spectrum, high reflectance values are characteristic of salt-affected soils (Mougenot and Pouget 1993). High reflectance values in the near- and mid-infrared spectrum have also been associated with soil salinity (Csillag et al. 1993).

For visual interpretation of salt-affected soils, false color composites (FCCs) are generated using three bands from a satellite sensor. Infrared bands are typically combined with visible bands with each band assigned to one of the primary colors, red, green, or blue. On certain false color composites, bright white colors are associated with high concentrations of salts on the soil surface (Nizeyimana and Peterson 1997). Although several studies have used

JERS (Japanese Earth Resources Satellite) and SPOT (Système Pour l'Observation de la Terre) satellites to detect soil salinity (Metternicht 1998; Rahman et al. 1994), most studies have used data from one or more of the Landsat satellites to generate FCCs.

Several Landsat band combinations have been used to generate FCCs for salinity studies. Bands 4, 3, and 2 from the Landsat Thematic Mapper (TM) sensor produce a FCC image on which bright white tones are associated with salt-affected soils (Sujatha et al. 2000; Verma et al. 1994; Rao et al. 1991). Other combinations include Landsat TM bands 4, 5, and 3 on which bright blue colors on the FCC image indicate salt-affected areas with little or no vegetation cover (Evans 1999). Salt-affected soils on bare ground appeared in red colors on a FCC image from Landsat TM bands 4, 5, and 7 (Evans et al. 1995).

In conjunction with ancillary data, remote sensing data are also used to detect different salt classes and estimate varying degrees of salt damage to soils. Using pH and electrical conductivity (EC) measurements from field soils samples, reflectance values from remote sensing data can be correlated with surface soil characteristics to map different types of salt classes, including saline, sodic, and saline-sodic soils (Metternicht and Zinck 1997; Sehgal and Sharma 1988). Quantitative analysis of tonal variations allows for detection of varying degrees of salinity and sodicity on false color composite images (Gore and Bhagwat 1991; Rao et al. 1991). A false color composite image using the first three principal components of a tasseled cap transformation on Landsat TM data facilitated discrimination of several salinity levels (Peng 1998).

Despite the utility of remote sensing data for detecting salt-affected soils, soil salinity and sodicity are complex processes influenced by soil conditions which may also affect reflectance characteristics, including soil grain size, soil moisture, organic matter and mineral

content (Hill 1994; Jensen 1996). In addition, reflectance values of salt-affected soils differ among FCCs since different spectral bands are combined to form each FCC image. As a result, the selection of bands and the soil conditions in a study area can limit the effectiveness of a FCC for distinguishing soil surface salinity. This study was conducted to compare four false color composites, in terms of the differences in mapping and detecting salt-affected soils. Specifically, this study has two objectives: (1) to analyze the ability of each false color composite to discriminate between different classes of salt-affected soils; and (2) to compare the spatial distributions of salt classes among the four false color composites: (a) false color composite using bands 4,3, and 2 (FCC 432); (b) false color composite using bands 4,5, and 3 (FCC 453); (c) false color composite using bands 4,5, and 7 (FCC 457); and (d) the first three principal components from the Tasseled Cap transformation on bands 1 through 5 and 7 (Tass. Cap 1,2,3).

MATERIALS AND METHODS

Study area

The study area is located in Kings County in the southwest portion of the San Joaquin Valley in California from 36° 00' to 36° 07' North and 119° 45' to 120° 00' West (Figure 1). The southern boundary is located about one-half mile north of Kettleman City. The study area encompasses 114 square miles of irrigated agricultural land. Cotton is the common crop, along with some wheat, alfalfa, and rice. Average annual precipitation ranges from 6 to 8 inches and average annual temperatures range from 63 to 65 degrees Fahrenheit, although average

maximum temperatures from July through September range from 90 to 96 degrees Fahrenheit (Arroues and Anderson, Jr. 1986).

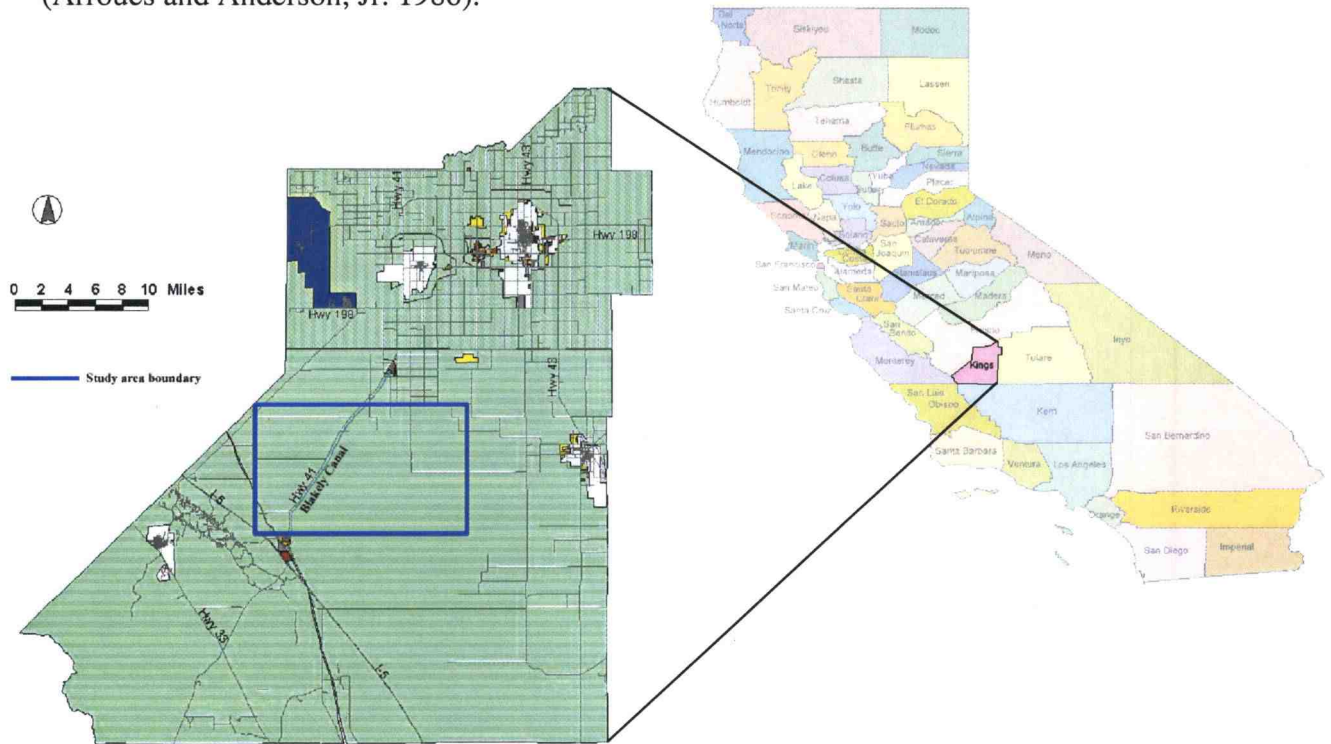


Figure 1. Location of study area within Kings County, California.

The study area is divided by Blakely Canal, which traverses the site in a northeast-southwest direction. This canal also divides two different soil geomorphologies east and west of the canal (Figure 1). To the east of Blakely Canal, the study area is located in a portion of the Tulare Lake Basin, containing alluvial and floodplain soils derived from igneous and sedimentary rock. Soils are Tulare clay, calcareous throughout the soil profile, and saline-sodic in some parts. This area is prone to long periods of flooding due to a perched water table created by an impermeable Corcoran clay layer 4 to 6 feet below the soil surface (Preston 1998). These conditions increase the rate of salinization since irrigation water that infiltrates through the soil profile remains perched a few feet below the

root zone. Through capillary action, this water is transported back to the root zone and soil surface with a higher salt concentration when subsurface salts are dissolved and transported to the surface in the soil water (Letey 2000). To decrease the rate of salinization in this portion of the study area, a subsurface drainage system network directs salty drainage water out of the soil profile and into surface evaporation ponds a few miles south of the study area (Arroues 2002, personal communication).

East of Blakely Canal, average elevation is 180 feet with 0 to 1 percent slopes (Arroues and Anderson, Jr. 1986). Approximately 84 square miles of the study area are located within the Tulare Lake Basin. The Kings River crosses the eastern portion of the study area in a north-south traverse. The Tule River intersects the Kings River in an east-west traverse.

West of Blakely Canal, the study area encompasses part of the alluvial fans originating from the Kettleman Hills range, forming the western boundary of the San Joaquin Valley. These alluvium soils are derived from sedimentary rock. Elevation ranges from 180 to 270 feet with 0 to 5 percent slopes. Approximately 30 square miles are located in this western portion of the study area. Predominant soils in this area are clay, loam, and clay loam with sandy loam inclusions in several map units. In some areas, soils are calcareous or saline-sodic.

Salinization in the San Joaquin Valley is contributing to the loss in productivity of 1.5 million acres per year (Preston 1998). Of particular concern is Kings County where salinization is exacerbated by its location within an internal drainage basin with areas containing poorly drained soils, and where areas in the western portion of the county have naturally high amounts of soluble salts (Preston 1998). The western coastal range of the San Joaquin Valley is composed of uplifted ocean floor sediments. Consequently, the soils originating along the

western portion of the valley naturally contain salts, especially selenium, which at high concentrations can be toxic to plants and other organisms (Ghassemi et al. 1995).

Image acquisition and pre-processing

Landsat 5 Thematic Mapper (TM) digital data obtained from Space Imaging, Inc., included orthorectified and georeferenced digital data (Table 1). The acquisition date was selected to correspond with the time of year when the study area contained the highest proportion of bare soil areas. In this study, only salt-affected areas on bare soil were considered in order to limit the number of complex variables that influence soil reflectance associated with surface salinity and sodicity. The satellite data were processed and analyzed using ERDAS Imagine, a digital image processing software system.

Table 1. Technical information for Landsat TM data used in this study.

Acquisition date	Path/Row	Projection	Datum	Ellipsoid	Pixel resolution
October 15, 1997	42/35	UTM Zone 11	NAD 83	GRS 80	25 meters

Four false color composite (FCC) images were generated using the following combinations: (1) Bands 4,3,2; (2) Bands 4,5,3; (3) Bands 4,5,7; and (4) the first three principal components of the Tasseled Cap transformation from bands 1,2,3,4,5, and 7. The first three principal components correspond to soil brightness, greenness, and wetness (Mather 1999). For each composite image, each band was matched to either the red, green, or blue color memory planes (Table 2).

Table 2. Landsat TM bands exposed to red, green, or blue color memory planes.

FCC image bands	Red	Green	Blue
4,3,2	4	3	2
4,5,3	4	5	3
4,5,7	4	5	7
Tass. Cap 1,2,3 (principal components)	1	2	3

Field sampling and soil analysis

The field data set consisted of 25 soil samples collected from the top 3 cm of the soil surface in April 2001 (Figure 2). Sample points were located fifty to one-hundred feet from the edge of each field. Field sampling locations were selected from areas exhibiting white and light blue-gray tones on FCC 432. Previous studies have associated these tonal characteristics with salt-affected soils (Rao et al. 1991; Verma et al. 1994). In order to classify crop areas in the image processing stage, two soil samples were also collected from areas showing crop growth on the FCC 432 image.

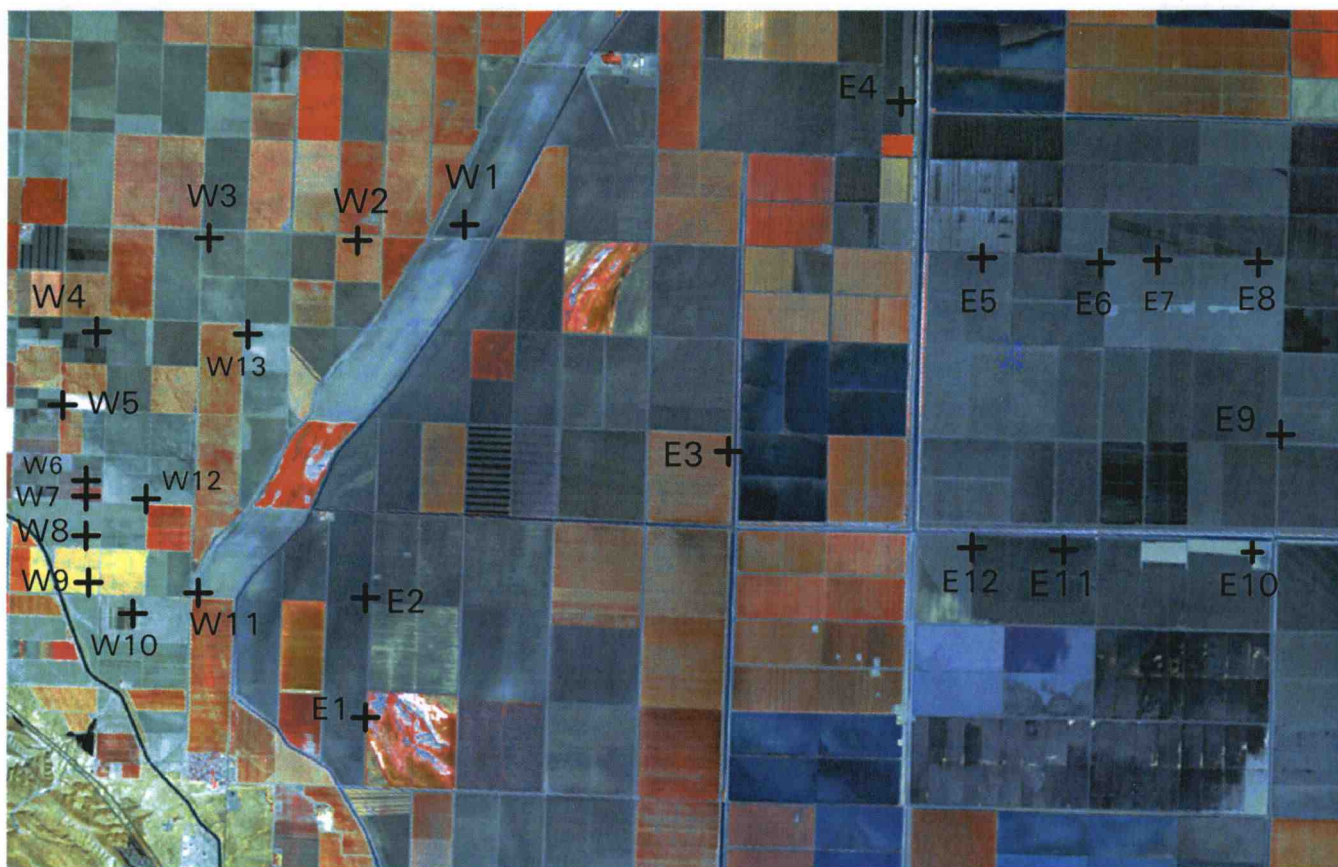
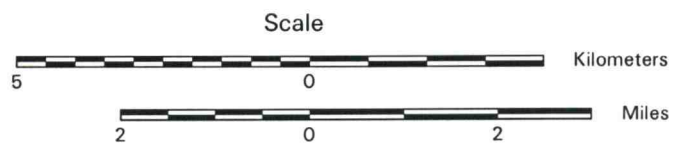


Figure 2. Location of field sample points mapped on a false color composite (FCC) image using Landsat TM bands 4,3, and 2.



Soil color was determined by comparing dry and wet soil samples to color chips on Munsell soil color charts. Soil texture was determined using the texture by feel method, in which percentages of sand, silt, and clay are estimated from moist soil samples subjected to different elasticity, plasticity and other texture tests. Soil pH, electrical conductivity (EC), and sodium adsorption ratio (SAR) were measured at the Central Analytical Lab at Oregon State University. Only thirteen soil samples were analyzed to determine their sodium adsorption ratio, which is an expensive soil analysis test. Concentrations of potassium, calcium, magnesium, and sodium are provided for those samples analyzed for SAR. Based on the laboratory data, five salt-affected soil classes were established for use in the supervised classification algorithm: Nonsaline (i.e., not salt-affected soils), slightly saline, saline, sodic, and saline-sodic. The distinction between saline, sodic, and saline-sodic soils is based on pH, EC, and SAR values (Table 3).

Table 3. Saline and sodic soil classes based on electrical conductivity (EC), pH, and sodium adsorption ratio (SAR), (Brady and Weil 1996).

Soil class	EC (mmhos/cm)	pH	SAR
Saline	> 4	< 8.5	< 13
Sodic	< 4	> 8.5	> 13
Saline-sodic	> 4	< 8.5	> 13
Slightly saline	3.6-3.9	<8.5	<13

Soil pH ranged from 7.6 to 8.6, while electrical conductivity ranged from 0.5 to 33.2 mmhos/cm. The highest electrical conductivity and sodium adsorption ratio measurements occurred in the saline-sodic soil samples. Eight samples were classified as salt-affected soils (Table 4).

Table 4. Chemical and physical characteristics of soil samples.

Sample	K	Ca	Mg	Na	EC	pH	SAR	Salt-affected class	Color		Texture
	ppm	-----meq/100g-----			mmhos/cm				dry	moist	
E1†‡	800	36.5	11.2	13	11.3	8.3	45.6	Saline-sodic	10YR 6/1	10YR 4/1	Clay
E2					1.5	8.3		nonsaline	10YR 5/1	10YR 4/1	Clay
E3‡					3.3	7.7		nonsaline	10YR 6/1	10YR 4/1	Clay
E4					3.9	8.1		Slightly saline	10YR 6/1	10YR 4/1	Clay
E5	747	36.4	12	2.8	2.9	8.0	9.7	nonsaline	10YR 6/1	10YR 4/1	Clay
E6‡					2.1	8.2		nonsaline	10YR 6/1	10YR 4/1	Clay
E7					1.8	8.2		nonsaline	10YR 6/1	10YR 4/1	Clay
E8‡	927	37.3	10.3	2.0	3.6	8.0	7	Slightly saline	10YR 6/1	10YR 4/1	Clay
E9					2.2	8.5		nonsaline	10YR 6/1	10YR 4/1	Clay
E10‡	1050	35.8	11.4	3.1	4.5	7.9	10.8	Saline	10YR 6/1	10YR 4/1	Clay
E11					1.8	8.4		nonsaline	10YR 6/1	10YR 4/1	Clay
E12‡	1080	34.9	11.4	2.3	1.4	8.5	15.4	Sodic	10YR 6/1	10YR 4/1	Clay
W1‡	492	17.5	7.4	2.7	2.7	8.6	13.3	Sodic	10YR 6/3	10YR 5/3	Clay
W2‡	626	15.8	6.6	1.8	3.5	8.2	9.5	nonsaline	10YR 6/3	10YR 5/3	Silty clay
W3					3.5	7.9		nonsaline	10YR 6/3	10YR 5/3	Clay
W4‡					2.2	8.1		nonsaline	10YR 6/3	10YR 5/3	Clay
W5‡	489	11.1	4.3	0.4	0.5	8.5	2.2	nonsaline	10YR 6/3	10YR 5/3	Sandy clay
W6					1.9	8.1		nonsaline	10YR 6/3	10YR 4/3	Sandy loam
W7‡	298	6.3	2.5	0.2	0.5	8.4	1.4	nonsaline	10YR 6/3	10YR 4/3	Sandy loam
W8‡					2.0	8.0		nonsaline	10YR 6/4	10YR 4/3	Sandy loam
W9‡	369	6.9	2.9	0.2	0.5	8.5	1.9	nonsaline	10YR 6/4	10YR 4/4	Sandy loam
W10‡	436	5.5	4.6	0.3	0.8	7.7	2.4	nonsaline	10YR 5/4	10YR 4/3	Sandy loam
W11‡	517	16.9	5.2	13.3	33.2	8.2	68.4	Saline-sodic	10YR 6/3	10YR 4/2	Silty clay
W12‡					1.8	7.6		nonsaline	10YR 6/3	10YR 4/3	Sandy clay
W13‡	556	18.1	5.9	1.6	3.9	8.5	8.2	Saline	10YR 6/3	10YR 4/3	Silty clay

† Samples E1-E12 located east of Blakely Canal; samples W1-W13 located west of Blakely Canal.

‡ Samples used to generate training signatures.

Saline, sodic, and saline-sodic soils are the three different types of salt-affected soils. Saline soils are characterized by high concentrations of neutral soluble salts, mainly chlorides and sulfates of sodium, calcium, magnesium, and potassium. High concentrations of these soluble salts restrict plant growth. Sodic soils are considered the most problematic in agriculture. Characterized by high concentrations of sodium ions, these soils greatly restrict plant growth due to the toxic levels of sodium, hydroxyl, and bicarbonate ions in the soil. Poor soil structure leading to a decrease in soil permeability is caused by the dispersion of soil colloids by sodium ions. Saline-sodic soils contain high levels of sodium ions and neutral soluble salts. Soil structure is not degraded as in sodium soils, however,

since the neutral soluble salts inhibit the dispersion of soil colloids otherwise caused by sodium ions (Brady and Weil 1996).

Classification of Landsat TM data

Image processing involved supervised training and classification. In supervised classification, prior knowledge about the study area is used in the classification algorithm. As a result, spectral characteristics such as tone, color, and pattern can be associated with land features to establish training sites. The training sites of different land feature classes are then used to train the classification algorithm in assigning pixels to classes in the remaining image (Jensen 1996). In ERDAS Imagine software, *training sites* were referred to as *signatures*. For consistency in this study, *training sites* are referred to as *signatures*.

In this study, signatures were determined from field sample points with various pH and EC values corresponding to different classes of salt-affected soils. Signatures were also established for the sandy soil samples, most of which exhibited high brightness values on all four FCC images. Sample W6 was excluded due to its high correlation with sample W7. During the classification process, the sandy soil samples (W5, W7, W8, W9, W10, and W12) were maintained as individual signatures. For display purposes, each classified FCC image was re-coded in order to merge all sandy soil signatures into one class value. To generate each signature, a neighborhood operator was created with a spectral Euclidean distance of 10, a geographic constraint of 300 pixels, and a nearest neighbor cross for each seed pixel.

The maximum likelihood classifier algorithm was used after signature histograms were checked for normal distribution. The maximum likelihood algorithm uses the mean,

variance, and covariance statistics of each signature to plot, in feature space, the distribution of pixels in each class. Concentric ellipses, based on increasing standard deviations, represent the probability of pixels being members of the class. The ellipses constructed from signature statistics are used to mathematically determine which class a pixel is assigned to. The mathematical criteria include the distance of each pixel to the center (mean) of the ellipse; and the orientation and dimensions of the major and minor axes of the ellipse (Mather 1999).

In an attempt to enhance spectral differences between classes, two digital image processing techniques were applied to the Landsat TM data; however, these techniques did not produce useful results. The first technique was applying a linear edge enhancement filter, which did not provide a significant difference in pixel values compared to the original Landsat TM data. The second technique involved surface texture analysis of band 6 data in order to distinguish between sandy soil and salt-affected soil classes. In band 6, sandy soils can exhibit a rough texture, while salt-affected soils display smooth textures (Verma et al. 1994). In this study, however, no visual differences in surface texture could be detected between sandy and salt-affected soil classes.

Comparison of false color composites

Since field reference data were not collected after classification of the false color composite images, overall accuracies could not be estimated. As a result, other image processing techniques were used to compare the classified images, including spectral profiles, signature separability data, and feature space images.

Different land features such as water, deciduous forest stands, and bare soil reflect and emit different amounts of electromagnetic energy, which also differ across the electromagnetic spectrum (Jensen 2000). Plotting the energy reflected as a function of wavelength for a certain land feature is called a *spectral signature* or, in Erdas Imagine, a *spectral profile*. In Erdas Imagine, spectral profiles were plotted across Landsat TM bands 1, 2, 3, 4, 5, and 7 for the different soil classes identified by using pixels coinciding with the soil sample locations. Plotting spectral signatures of different classes on one graph allowed for comparisons of spectral characteristics between salt-affected soils and other classes.

One key procedure in classifying images is determining the optimum combination of bands that give the maximum spectral separation between two classes. In doing so, classification errors are minimized. In ERDAS Imagine, the process of evaluating the degree of separability between the signatures of each class is termed *signature separability*. In this study, signature separability data were determined using the transformed divergence calculation, which adjusts for any weighting that can result between classes that could over-inflate the divergence value (Jensen 1996).

One visual method for evaluating the degree of separability between signatures is plotting ellipses for each signature in two-dimensional feature space. These ellipses are generated using mean and standard deviation statistics for each training signature. Poor signature separability is present when ellipses are closely spaced or overlapping, while non-overlapping ellipses located in different regions of the feature space will have good signature separability (Jensen 1996). In this study, each false color composite image was used as input data to generate four feature space plots. Salt-affected signatures from each

FCC were draped over each corresponding feature space plot. The third standard deviation was used when plotting all signature ellipses.

RESULTS AND DISCUSSION

Preliminary comparison of false color composites

A visual comparison of the four false color composite images revealed that bright white and dull white patches on FCC 432 corresponded to white and light blue-gray or light green tones on FCC 453 and FCC 457; and corresponded to red and bright red tones on the Tasseled Cap image (Figure 3). Red, green, and blue colors on the Tasseled Cap image correspond to varying degrees of brightness, greenness, and wetness, respectively (Jensen 1996). Brightness is associated with bare soil reflectance and has been used to detect salt-affected surface soils (Peng 1998). Greenness corresponds to areas with vegetation while wetness, or the degree of soil moisture, is depicted in varying degrees of blue tones. Since the eastern portion of the study area is prone to flooding, the Tasseled Cap image provides a useful visual index for detecting areas containing high soil moisture regimes. Due to a perched water table in the eastern portion of the study area, dark blue colors on the Tasseled Cap image may indicate areas at higher risk for salinization.

Six soil samples (E1, E10, E12, W1, W11, and W13) whose location exhibited high brightness values on the false color composites were either saline, sodic, or saline-sodic (Table 4). Sample E12 was sodic and appeared to have a lower brightness value compared to the other salt-affected samples on all four false color composites (Figure 3). Two soil

samples (E4 and E8) were categorized as slightly saline (Table 4). Sample E8 displayed higher brightness values than sample E4 on all four composites (Figure 3), even though sample E4 had a slightly higher EC value (Table 4). The best spectral distinction between samples E4 and E8 was in the Tasseled Cap image, in which a dull red color marks the location of sample E8, while a blue color with dull red tones is found at the location of sample E4 (Figure 3d).

The rectangular pattern of the area surrounding soil sample E10 is not characteristic of the salinization process (Figure 3; refer to Figure 1 for sample locations). The pattern is likely due to a land management practice, quite possibly the application of gypsum, which also has high reflectance values in Landsat TM bands 1 through 5 (Mougenot and Pouget 1993). Gypsum is applied to sodic and saline-sodic soils to decrease high sodium concentrations (Brady and Weil 1996). Sample E10 was classified as saline and may indicate the existence of previous saline-sodic soil conditions. An application of gypsum would have decreased the amount of sodium in the soil, resulting in the current classification of the soil sample as saline.



(a) TM Bands 4, 3, 2 = RGB



(b) TM Bands 4, 5, 3 = RGB

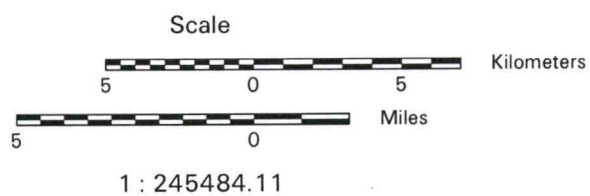


(c) TM Bands 4, 5, 7 = RGB



(d) First three principal components of Tasseled Cap transformation: 1, 2, 3 = RGB

Figure 3. Color composites of Landsat Thematic Mapper data for the study area. (a) Composite of TM bands 4, 3, and 2 placed in the red, green, and blue (RGB) image processor memory planes, respectively. (b) TM bands 4, 5, and 3 (RGB). (c) TM bands 4, 5, and 7 (RGB). (d) First three principal components of the Tasseled Cap transformation 1, 2, and 3 (RGB). Note light blue color patches in (b) and (c) coincide with light green patches in (a) and with bright red patches in (d).



Interpretation of spectral profiles

Spectral profiles of the different salt-affected soils revealed higher brightness values for saline soils compared to sodic and saline-sodic soils (Figure 4). Sodic soils had the lowest brightness values across the visible and infrared spectrum. Higher brightness values for saline soils were also exhibited in the first principal component of the Tasseled Cap transformation (Figure 5).

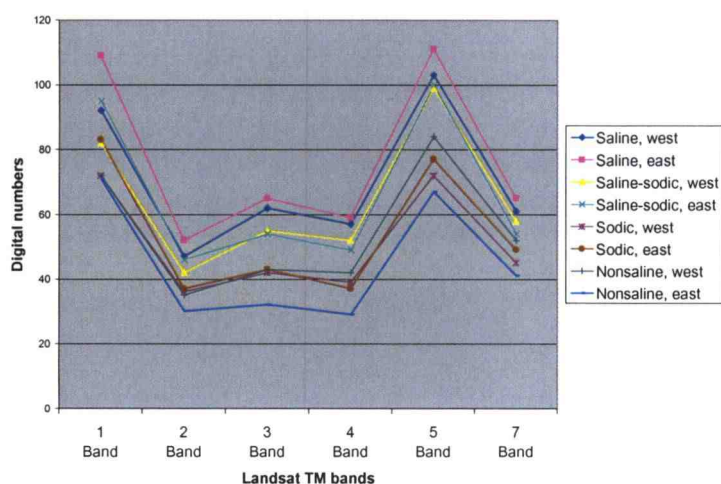


Figure 4. Spectral profiles of salt-affected and nonsaline soils.

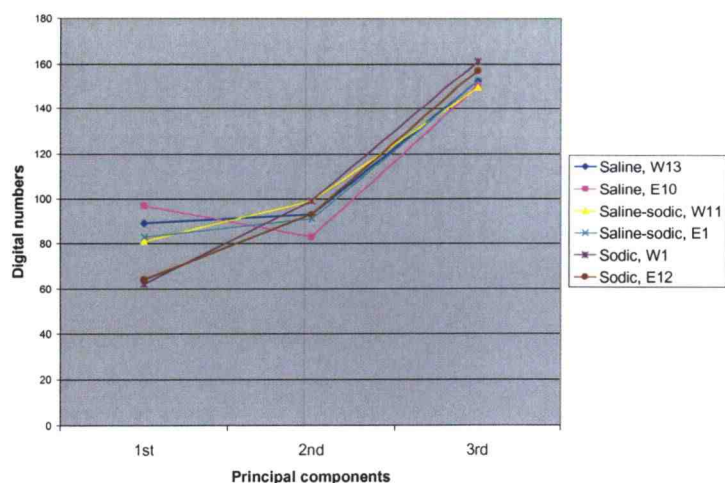


Figure 5. Spectral profiles of salt-affected soils along the first three principal components of the Tasseled Can transformation.

Six samples (W5, W6, W7, W9, W10, and W12) exhibiting bright tones on the false color composites were not salt-affected soils (Table 4). A possible explanation for the high brightness values was the high sand content in all six soils as determined through texture by feel (Table 4) and confirmed with soil survey information (Arroues and Anderson, Jr. 1986). In comparison to other soil textures, sandy soils exhibit high reflectance values across the visible and infrared portions of the electromagnetic spectrum (Mougenot and Pouget 1993).

In this study, three of the sandy soil samples (W6, W10, and W12) exhibiting bright tones on the composite images had similar spectral profiles as the saline and saline-sodic soils, with higher brightness values than sodic and nonsaline soils (Figure 6).

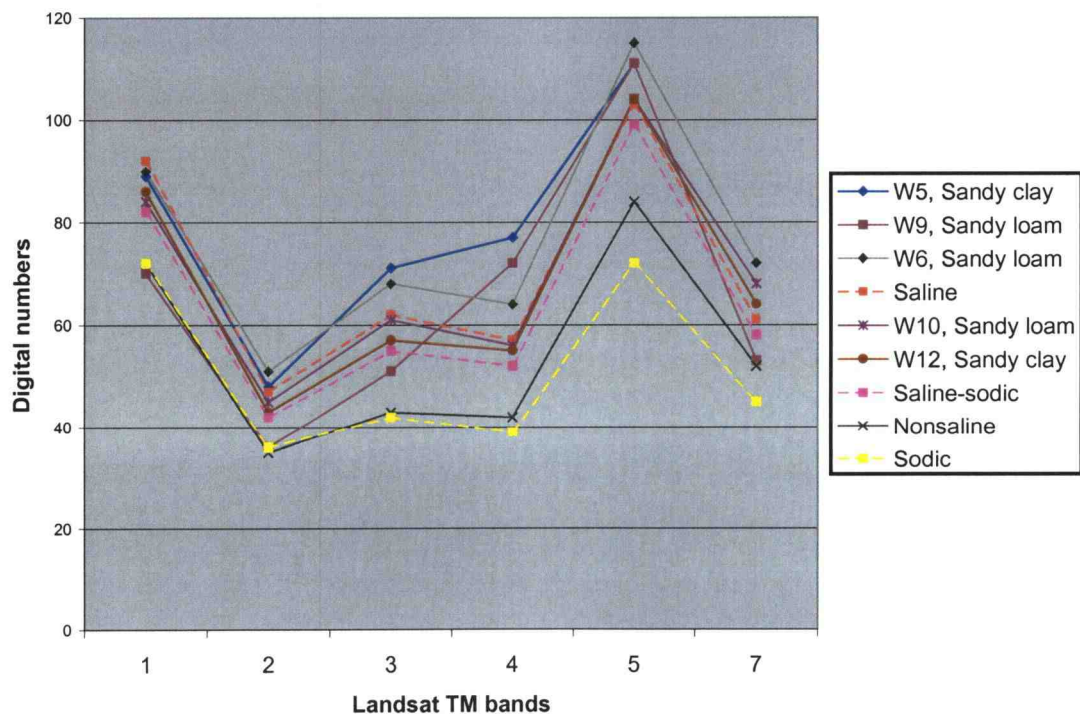


Figure 6. The spectral profiles of salt-affected and sandy soils from soil samples in the western portion of the study area.

Two soil samples, W5 and W9, displayed unique spectral profiles, in which brightness values increased from band 3 to band 4, whereas values decreased from bands 3 to 4 for all other soil samples (Figure 6). This unique characteristic could not be explained by differences in soil color or texture; both samples (W5 and W9) have soil colors and textures which are similar to the other sandy soil samples that did not exhibit this unique spectral profile pattern (Table 4). However, a visual inspection of the four composite images does reveal unique colors for soil samples W5 and W9 in comparison to other sandy soil areas exhibiting bright tones. In FCC 457, for example, bright tan colors distinguish the areas of samples W5 and W9 from the bright white and light blue colors of the other sandy soil samples (Figure 3c; refer to Figure 1 for sample locations). In the Tasseled Cap image, the W9 sample area is bright orange as opposed to the red colors of the other sandy soils nearby (Figure 3d). Due to the rectangular pattern of these two unique patches from which samples W5 and W9 were taken, it is quite possible that their unique spectral brightness patterns across bands 3 and 4 are a result of some land use management practice.

The similarity in brightness values between sandy soils and salt-affected soils illustrates one of the challenges in using remotely sensed data for detecting soil salinity. Several chemical and physical characteristics of soils influence soil reflectance, including mineral composition, amount of hygroscopic water, soil texture, organic matter and soil moisture (Ben-Dor et al. 1999). It is this soil variability that emphasizes the importance of selecting FCC's for soil salinity studies based on the soil characteristics of a given area.

Comparison of classified images

The maximum likelihood classification algorithm applied to each false color composite image produced visible differences in the number of pixels assigned to each class (Figure 7). The classification based on the Tasseled Cap data assigned the greatest number of pixels to the sandy soil class while the FCC 457 classified image had the greatest area classified as sodic soils (Figure 7). The highest saline-sodic areas were mapped in FCC 453 and FCC 457 while the largest area classified as slightly saline was mapped in FCC 432. The FCC 457 contained the lowest classified area of nonsaline soils (Figure 7).

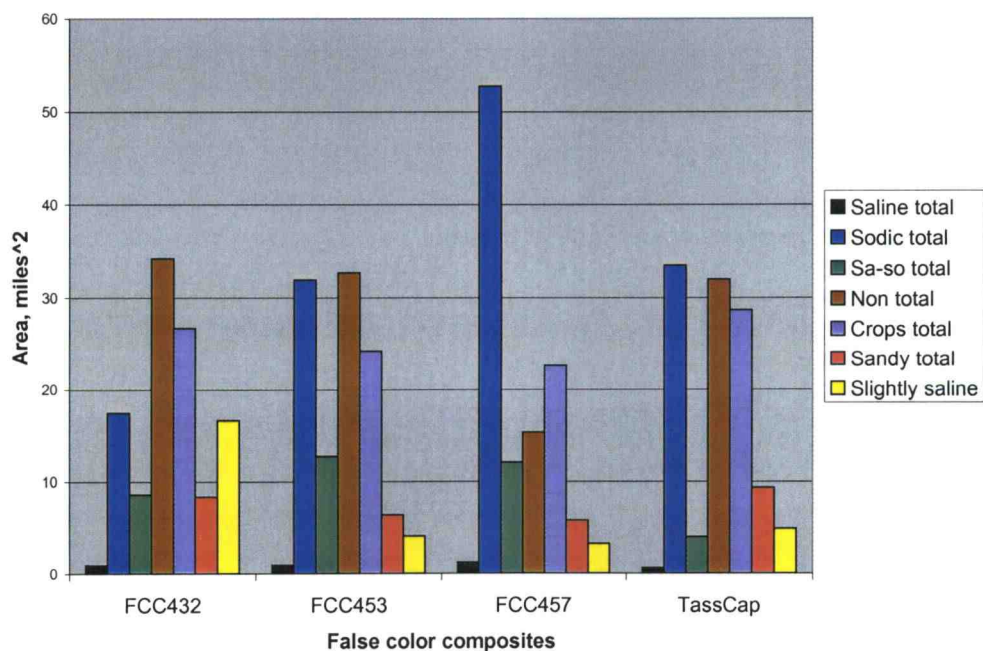
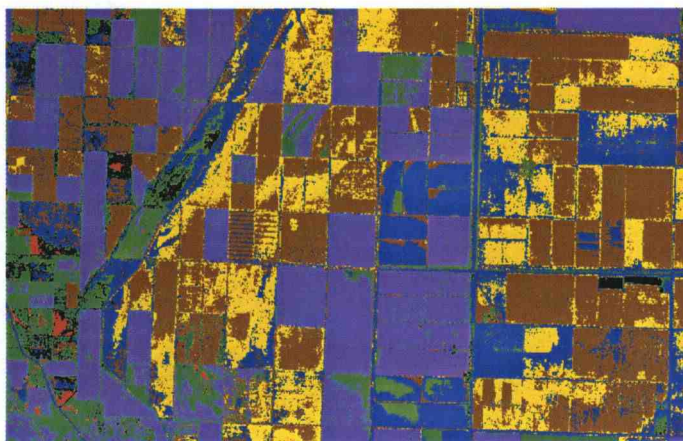


Figure 7. Total area per class for each false color composite.

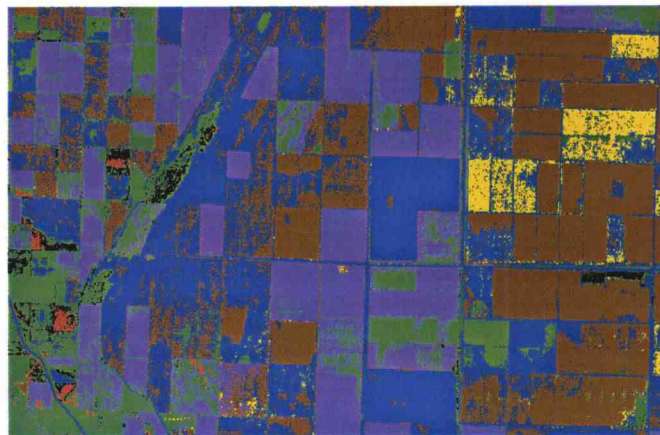
East of Blakely Canal, several pixels were classified as sandy soils in all four classified images (Figure 8). However, no sandy soil textures exist approximately 1 to 3 miles east of Blakely Canal in this portion of the study area, as confirmed by the soil texture by feel method and soil survey information (Arroues and Anderson, Jr. 1986). In this study, allowing the sandy soil signatures to serve as training data for the entire study area illustrates the problem of inaccuracy resulting from extending signatures into geographic areas that may not be representative of the training data (Jensen 1996).

It is possible that classification accuracy would improve if training data from sandy soil samples were confined to the area west of Blakely Canal, where sandy loam mapping units and sandy loam inclusions exist. Even so, a visual inspection of the classified images reveals pixels classified as salt-affected soils in areas within close proximity to sandy soil samples. Only by collecting post-classification soil samples as reference data can the accuracy of these classified pixels be determined. Since no reference data were collected in this study, the ability of each false color composite to distinguish between salt-affected soils and sandy soils was analyzed using signature separability data.

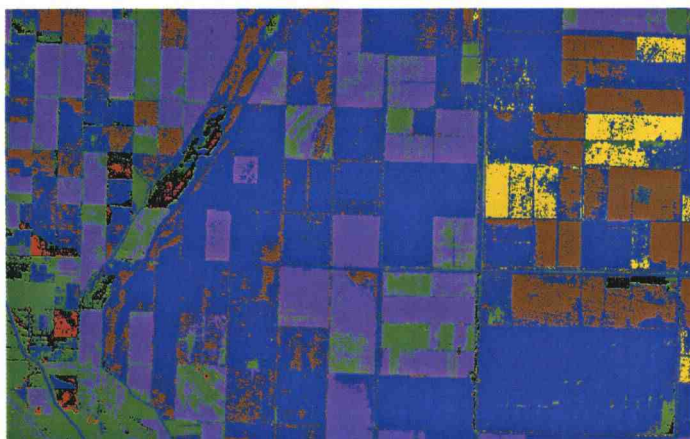
As previously discussed, transformed divergence values indicate the degree to which a pair of signature classes are spectrally different from one another within a set of one or more bands. Transformed divergence values are divided into ranges that indicate the quality of separability between classes (Table 5).



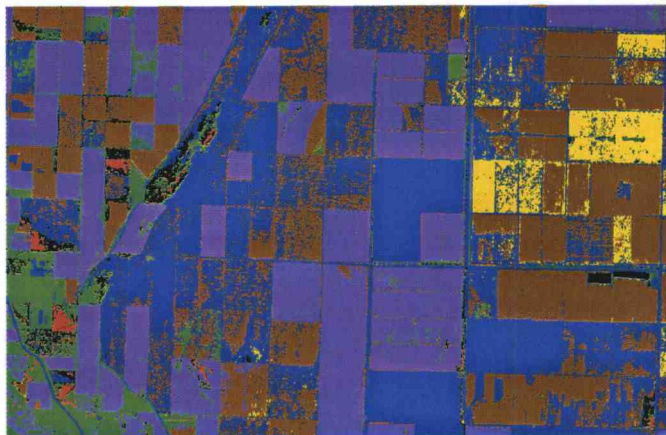
(a) FCC 432



(b) FCC453



(c) FCC 457



(d) Tasseled Cap 1, 2, 3

Figure 8. Maximum likelihood classification algorithm applied to training data from the Landsat TM image. (a) Composite of TM bands 4, 3, and 2. (b) TM bands 4, 5, and 3. (c) TM bands 4, 5, and 7. (d) First three principal components of the Tasseled Cap transformation 1, 2, and 3.

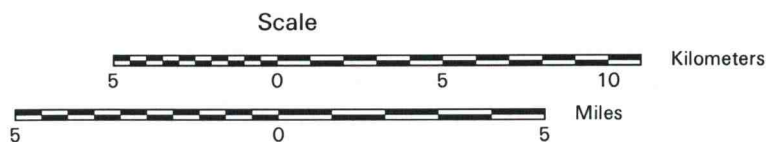
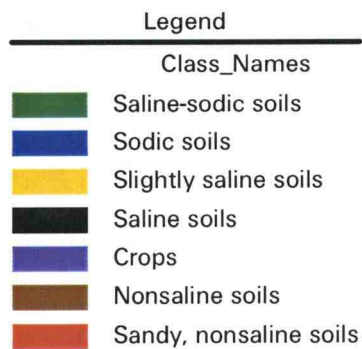


Table 5. Quality of separability defined by ranges in transformed divergence values (Jensen 1996).

Value range	Quality of separability
2000(maximum value)	Excellent
1900-1999	Good
<1700	Poor

Since sandy soil classes were located west of Blakely Canal, these classes were compared only to salt-affected soil classes located to the west of Blakely Canal. A wide variability in transformed divergence values occurred between the sandy soil and salt-affected soil signatures (Figure 9). Values of 2000 occurred between salt-affected soil signatures (saline, sodic, and saline-sodic) and sandy soil signatures, W5 and W9, in all four false color composite images (Figure 9). Poor separability (transformed divergence values < 1617) between sandy soil signatures, W7, W10, and W12, and saline signatures occurred in all four false color composites. The bright tones and light blue colors of these three sandy soil samples are visually similar to the brightness tone and color of saline sample, W13, in all four false color composites (Figure 3). This spectral similarity is confirmed by the low transformed divergence values between the saline and sandy soil signatures. Poor separability occurred between the saline-sodic signature and sandy soil signatures, W10 and W12, in all four false color composites. Excellent and good separability occurred between the sodic signature and sandy signatures, W5, W7, W9, W10, and W12, for all false color composites. As illustrated in the spectral profile graphs, the sodic classes had lower brightness values than the sodic and saline-sodic classes across all bands, while most of the sandy classes exhibited brightness values that more closely resembled those of the saline and saline-sodic classes. As a result, separability values between the sodic signature and most sandy soil signatures are higher than values between the saline/saline-sodic signatures and most of the sandy soil signatures (Figure 9).

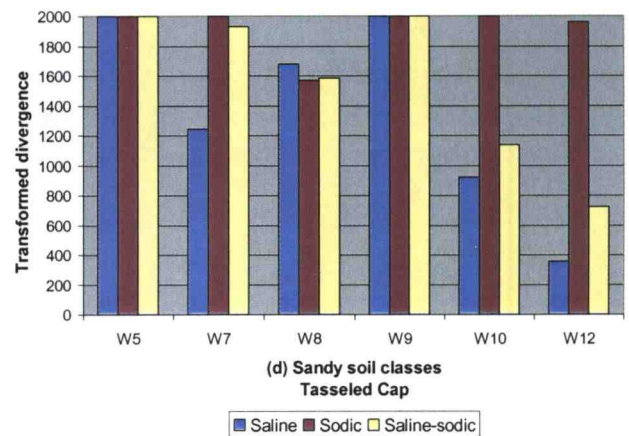
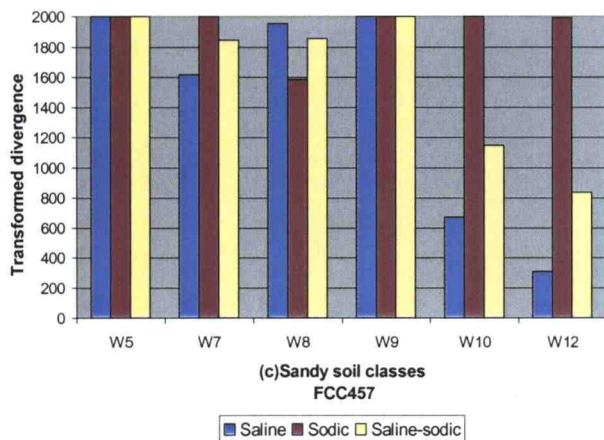
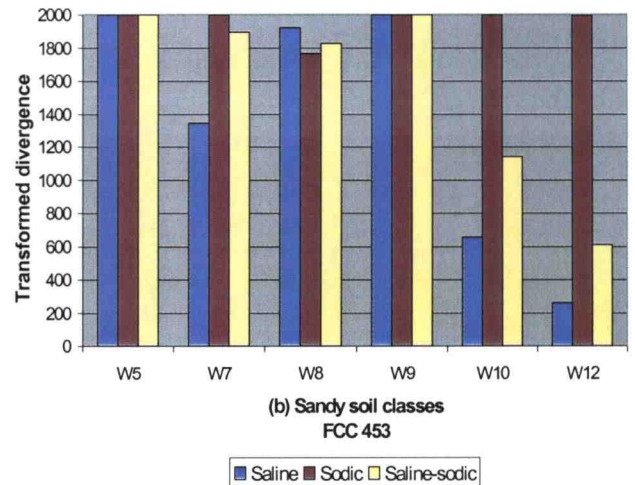
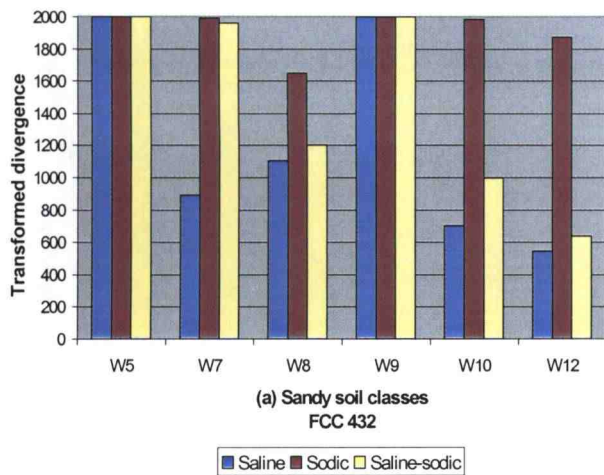


Figure 9. Transformed divergence values between sandy soil signatures and salt-affected soil signatures. All signatures are from portion of study area that is west of Blakely Canal.

The wide variability in transformed divergence values exhibited within each FCC indicates the spectral variability that exists within sandy soil classes, including those with similar soil textures. For example, signatures W7, W8, W9, and W12 are sandy loams (Arroues and Anderson, Jr. 1996), however, transformed divergence values between each signature and the same salt class varies from excellent to poor within each false color composite image (Figure 9). Perhaps other soil characteristics are masking or enhancing the soil reflectance of the sandy soil signatures, which again illustrates the complexity of soils and the potentially numerous soil variables that can influence soil reflectance values.

No false color composite image provided good separability between all the sandy signatures and the salt-affected signatures. With the exception of signature W8, transformed divergence values greater than 1800 occurred between the same pairs of sandy soil and salt-affected soil signatures in all four false color composites. Transformed divergence values less than 1700 (poor separability) occurred between the same pairs of sandy soil and salt-affected soil signatures in all four false color composites, with the exception of signature W8 (Figure 9). Good separability between sandy soil signature, W8, and the saline signatures was achieved by FCC 453 and FCC 457 (Figures 9b and 9c), which surpassed values in FCC 432 and the Tasseled Cap composite (Figures 9a and 9d).

For salt signatures in the western portion of the study area, excellent separability (transform divergence > 1990) occurred between the sodic and saline or saline-sodic signatures, while poor separability (transformed divergence values < 1548) occurred between saline and saline-sodic classes for each false color composite (Figure 10). Poor separability (transformed divergence values < 1680) also occurred between the nonsaline and sodic signatures for each false color composite (Appendix).

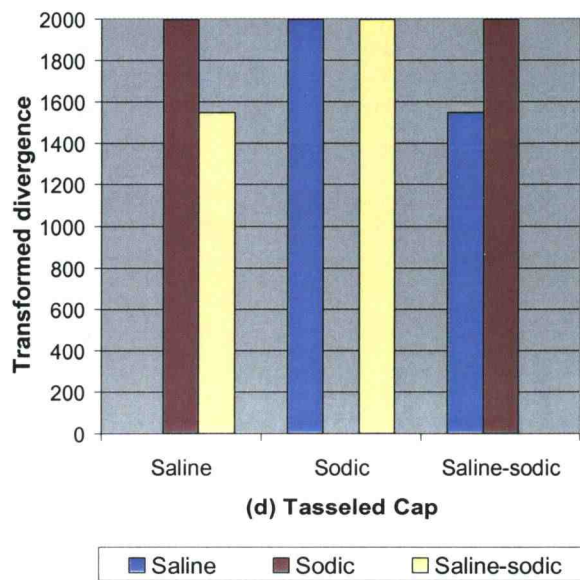
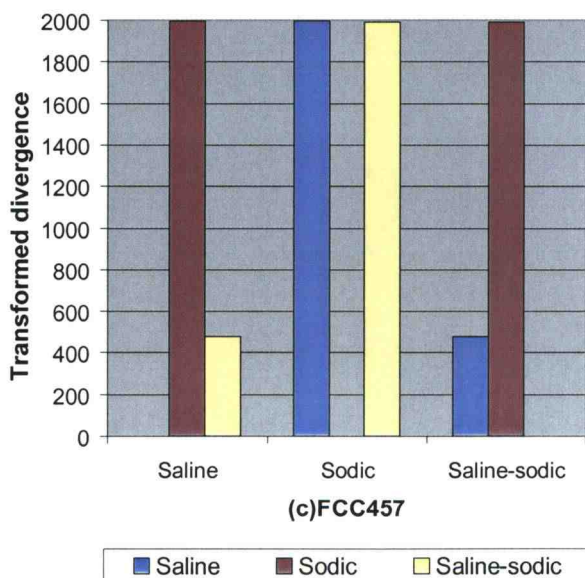
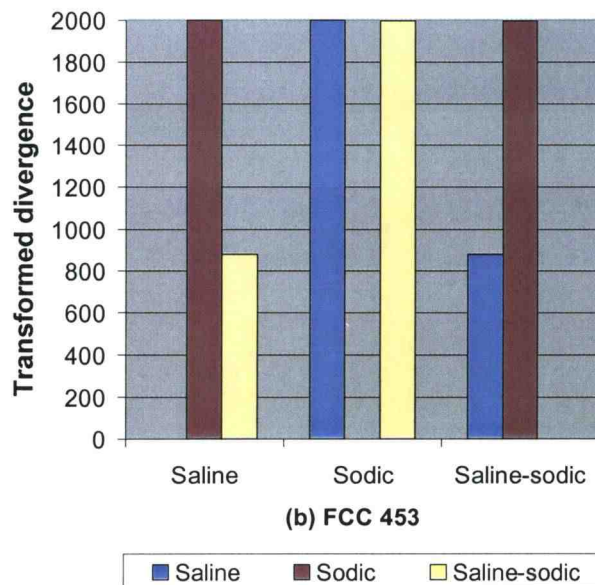
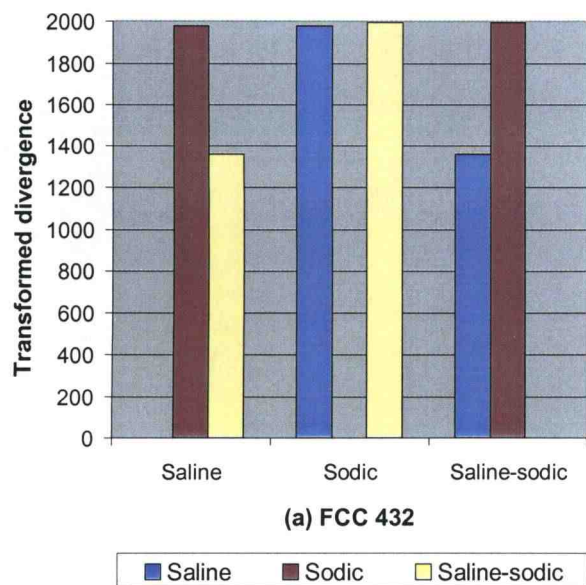
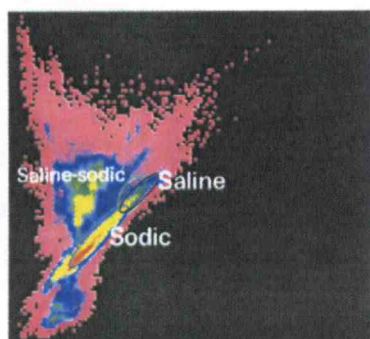


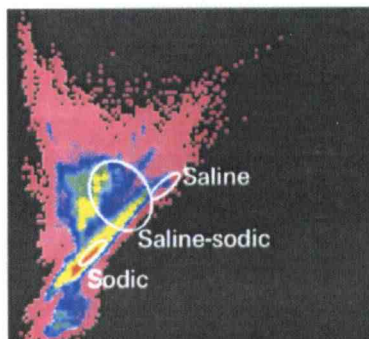
Figure 10. Transformed divergence values between salt-affected signatures. All signatures are from the portion of the study area that is west of Blakely Canal.

For salt signatures in the eastern portion of the study area, excellent separability (transformed divergence values = 2000) occurred between all salt signatures, except between the sodic and slightly saline signatures, which exhibited poor separability (Appendix). FCC 457 exhibited good and excellent signature separability between nonsaline and sodic signatures and between nonsaline and slightly saline signatures, respectively. Poor separability values occurred between all but one of these signature pairs in the other false color composites (Appendix).

Differences in separability between salt signatures were evident by plotting signatures in feature space. Feature space plots using several band combinations show little or no overlap between the saline and sodic signatures (Figure 11). For salt signatures from the eastern study area, little or no overlap occurred, which corresponds with the high divergence values between salt signatures from the eastern study area. In the western study area, a high degree of overlap occurred between saline-sodic and saline signatures (Figure 11).



Western study area

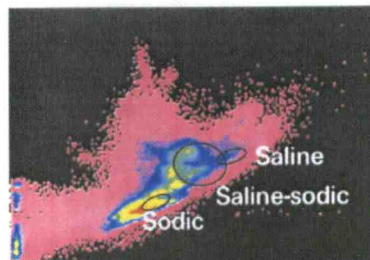


Eastern study area

FCC 432
Bands 3 and 4
(x, y axes, respectively)

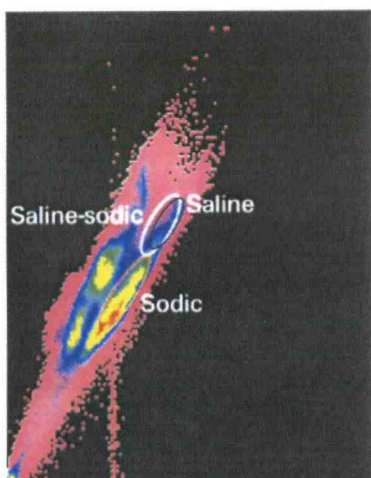


Western study area

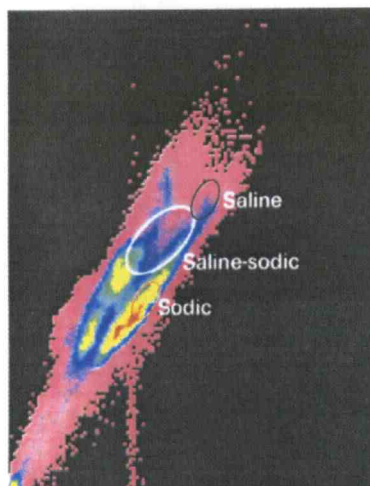


Eastern study area

FCC 453
Bands 5 and 4
(x, y axes respectively)



Western study area



Eastern study area

FCC 457
Bands 7 and 5
(x, y axes, respectively)



Western study area



Eastern study area

Tasseled Cap
1st and 3rd principal
components
(x, y axes, respectively)

Figure 11. Salt-affected soil signatures plotted on the feature space of several bands for each false color composite.

CONCLUSIONS AND RECOMMENDATIONS

The results of this study indicate that all four false color composites were similar in their ability to discriminate among salt-affected soils and between sandy soils and salt-affected soils. Good or poor separability values among the different classes were relatively similar among the four FCCs. For example, all four FCCs produced greater separability between sodic and most of the sandy soil classes, whereas lower separability values between saline/saline-sodic classes and most sandy soil classes occurred in all four FCCs. Differences in separability values between the east and west portions of the study area were also similar in all four FCCs.

Greater separability occurred between salt-affected soils in the eastern portion of the study area than in the area west of Blakely Canal where the presence of sandy soil inclusions limited the discrimination of salt-affected soils. East of Blakely Canal, good separability occurred among all salt-affected soil signatures (saline, sodic, and saline-sodic), except between the sodic and slightly saline soils. In the western portion of the study area, spectral similarities between sandy soils and saline/saline-sodic soils decreased signature separability in all four false color composites which indicated limited capabilities by all four composites to accurately distinguish between saline/saline-sodic soils and soils with high sand content. In the west, poor signature separability also limited the ability to discriminate between saline and saline-sodic soils in all four false color composites. Distinguishing between nonsaline and sodic soils is also limited in all four false color composites with the exception of soil samples east of Blakely Canal in FCC 432, FCC 453, and FCC 457.

Poor distinction between saline and saline-sodic soils in the western study area poses a challenge in using remotely sensed data to map salt-affected soils. Since different management practices are applied to saline and saline-sodic soils, appropriate use of remotely sensed data would require substantial ground truthing data to ensure accurate discrimination between saline and saline-sodic soils in the western portion of the study area. Greater temporal and spectral resolution may improve discrimination between salt-affected soils. Future studies in this area may incorporate remote sensing data from different seasons in order to provide better discrimination between sandy soils and salt-affected soils. One caveat, however, is that data must be limited to Landsat scenes in which the maximum spatial extent of bare soil exists in order to measure brightness or reflectance values from surface soils. In agricultural areas, this window of time may be limited. As such, seasons that are optimal for discriminating between sandy and salt-affected soils may not be available for study if the time period corresponds with peak crop growth. Crop calendars could be used to select time periods with minimum crop growth. Another limiting factor in selecting multiple-date satellite scenes is that the dry season is optimal for detecting surface salt since high evaporation rates during this time increase salt concentrations at the soil surface (Brady and Weil 1999). Increasing the spectral resolution by using more than three Landsat TM bands may improve discrimination between salt-affected soils. In one study, the highest separability between salt-affected soil classes was achieved using six combined Landsat TM bands (Metternicht and Zinck 1997). Due to differences in separabilities between east and west portions of the study area, future remote sensing research will require separate classification processes for areas east and west of Blakely Canal.

Based on signature separability data, no false color composite provided an overall improvement in discriminating between soil classes compared to the other false color composites. This may indicate a limitation not in the selection of bands, but perhaps in a limited spectral resolution of Landsat TM bands for distinguishing among salt-affected soil classes and sandy soils in this particular study area. In two separate studies, narrow spectral ranges were identified as providing better discrimination of saline soils than waveband ranges on current satellite sensors, including Landsat TM and SPOT satellite sensors (Hick and Russell 1990; Csillag et al. 1993). In this study area, narrower spectral bands may provide the ability to distinguish between salt-affected soils and saline/saline-sodic soils. To determine if narrower wavebands would provide better discrimination, a field spectrometer could be used to measure reflectance in areas containing sandy soil inclusions and salt-affected soils within close geographic proximity.

Two false color composites provided a few improvements in discriminating between soil classes. FCC 453 and FCC 457 achieved good separability between sandy soil signature, W8, and the saline signature, whereas FCC 432 and the Tasseled Cap composite provided poor separability. FCC 457 was the only composite that had good and excellent separability between nonsaline and sodic or slightly saline signatures in the eastern portion of the study area.

Differences in the number of pixels assigned to each class among the four false color composites underscore the need for post-classification reference data to estimate classification accuracy in each false color composite. The greatest difference occurred in FCC 457, which contained the largest area classified as sodic soils within the FCC 457 image and among the other three false color composites. All four composites exhibited a

signature extension problem, as several pixels in the eastern study area were classified as sandy soil in each false color composite. Results of this study also indicate that prior knowledge of land use practices in this study area may improve the mapping of salt-affected soils. Land use practices, such as the application of gypsum, may interfere with the reflectance characteristics of sodic and saline-sodic soils. Knowledge of such land use practices can help distinguish between reflectance values due to gypsum and those caused by the presence of salts in the soil surface. In this study area, subsurface drainage of salt water is used to decrease salt concentrations in soils that are most sensitive to salinization. Knowledge of these locations could be used during the classification phase by assigning different probability weights to fields that are drained of salt water, thereby improving the accuracy of mapping.

The research design in this study includes components that either proved useful or may need improvements in future research of this study area. Transformed divergence values and spectral profiles were two components that facilitated image analysis and the comparison of FCCs. A few components of the research design were limited, however. Lack of a sampling design contributed to a biased selection of sampling points, which limits the reliability of the results. In addition, collection of sampling points at the edge of fields may not be representative of salinization in the interior of fields. Location of sampling points from the interior of fields could be selected using a sampling design such as stratified random sampling. A greater number of samples should be established in future research of this study area. The limited number of samples in this study may not have accurately represented the spectral signatures of salt-affected soils nor accurate evaluation of separability between salt-affected soil classes and between sandy soils and salt-affected

soil classes. Last, a comparison of false color composites was limited without the use of statistics or post-classification reference data.

The low discrimination between several soil types and salt-affected soils using remote sensing data illustrates the challenge in mapping salt-affected soils. Soil ecosystems are dynamic and complex. As a result, various soil characteristics, including soil texture, can enhance or mask the reflectance values of salt-affected soils. This presents the researcher with a formidable task; but a crucial one, if remote sensing applications are to contribute to the mapping and management of salt-affected soils.

REFERENCES

- Arroues, K. and C.H. Anderson, Jr. 1986. *Soil Survey of Kings County, California*. USDA-SCS. Washington, D.C.: U.S. Gov. Printing Office.
- Barrett, E.C. and M.G. Hamilton. 1986. Potentialities and problems of satellite remote sensing with special reference to arid and semiarid regions. *Climatic Change* 9:167-186.
- Ben-Dor, E., J.R. Irons, and G.F. Epema. 1999. Soil reflectance. In *Remote Sensing for the Earth Sciences: Manual of Remote Sensing*, ed. A.N. Rencs, 111-188. 3rd ed. Vol. 3. New York: John Wiley and Sons.
- Brady and Weil. 1996. *The Nature and Properties of Soils*. 12th ed. New Jersey: Prentice Hall.
- Csillag, F., L. Pasztor, and L.L. Biehl. 1993. Spectral band selection for the characterization of salinity status of soils. *Remote Sensing of Environment* 43(3):231-242.
- Dwivedi, R.S. and K. Sreenivas. 1998. Image transforms as a tool for the study of soil salinity and alkalinity dynamics. *International Journal of Remote Sensing* 19(4):605-619.
- Dwivedi, R.S., K. Sreenivas, and K.V. Ramana. 1999. Inventory of salt-affected soils and waterlogged areas: a remote sensing approach. *International Journal of Remote Sensing* 20(8):1589-1599.
- Evans, F.H., P.A. Caccetta, R. Ferdowsian, H.T. Kiiveri, and N.A. Campbell. 1995. Predicting salinity in the Upper Kent River catchment. Report to LWRD. CSIRO Division of Mathematics and Statistics, Perth.
- . 1999. CSIRO, Mathematical and Information Sciences: Mapping and Monitoring Salinity. <http://www.cmis.csiro.au/rsm/casestudies/flyers/mapsal/index.htm> (March 16, 2001).
- Ghassemi, F., A.J. Jakeman, and H.A. Nix. 1995. *Salinisation of land and water resources*. Australia: University of New South Wales Press, Ltd.
- Gore, S.R., K.A. Bhagwat. 1991. Saline degradation of Indian agricultural lands: A case study in Khambhat Taluka, Gujarat State (India), using satellite remote sensing. *Geocarto International* 6(3):5-13.
- Hick, P.T. and W.G.R. Russell. 1990. Some spectral considerations for remote sensing of soil salinity. *Australian Journal of Soil Research* 28(3):417-431.
- Hill, J. 1994. Spectral properties of soils and the use of optical remote sensing systems for soil erosion mapping. In *Chemistry of Aquatic Systems: Local and Global Perspectives*, ed. G. Bidoglio and W. Stumm, 497-526. Netherlands: ECSC.

Jensen, R. R. 1996. *Introductory Digital Image Processing: A Remote Sensing Perspective*. 2nd ed. New Jersey: Prentice Hall.

Jensen, R.R. 2000. *Remote Sensing of the Environment: An Earth Resource Perspective*. New Jersey: Prentice Hall.

Kalra, N.K. and D.C. Joshi. 1996. Potentiality of Landsat, SPOT, and IRS satellite imagery for recognition of salt affected soils in Indian Arid Zone. *International Journal of Remote Sensing* 17(15):3001-3014.

Kaushalya, R. 1992. Monitoring the impact of desertification in western Rajasthan using remote sensing. *Journal of Arid Environments* 22:293-304.

Kumar, M., E. Goossens, and R. Goossens. 1993. Assessment of sand dune change detection in Rajasthan (Thar) Desert, India. *International Journal of Remote Sensing*. 14(9): 1689-1703.

Letey, J. 2000. Soil salinity poses challenges for sustainable agriculture and wildlife. *California Agriculture* March-April 2000.

Mather, P.M. 1999. *Computer processing of remotely-sensed images: An introduction*. 2nd ed. New York: John Wiley and Sons.

Metternicht, G. 1998. Fuzzy classification of JERS-1 SAR data: An evaluation of its performance for soil salinity mapping. *Ecological Modelling* 111:61-74.

Metternicht, G.I. and J.A. Zinck. 1997. Spatial discrimination of salt- and sodium-affected soil surfaces. *International Journal of Remote Sensing* 18(12):2571-2586.

Mishra, J.K., M.D. Joshi, and R. Devi. 1994. Study of desertification process in Aravalli environment using remote sensing techniques. *International Journal of Remote Sensing* 15(1):87-94.

Mougenot, B. and M. Pouget. 1993. Remote sensing of salt affected soils. *Remote Sensing Reviews* 7:241-259.

Nizeyimana E. and G.W. Petersen. 1997. Remote sensing application to soil degradation assessments. In *Methods for Assessment of Soil Degradation*, ed. Lal, R., W.H. Blum, C. Valentine, and B.A. Stewart, 393-403. New York: CRC Press.

Peng, W. 1998. Synthetic analysis for extracting information on soil salinity using remote sensing and GIS: a case study of Yanggao Basin in China. *Environmental Management* 22(1):153-159.

Preston, W. 1998. "Irrigated Agriculture." California Polytechnic State University, San Luis Obispo, 26 Feb. 1998.

Rahman, S., G.F. Vance, and L.C. Munn. 1994. Detecting salinity and soil nutrient deficiencies using SPOT satellite data. *Soil Science* 158(1):31-39.

Rao, B.R.M., R.S. Dwivedi, L. Venkataratnam, T. Ravishankar, and S.S. Thammappa. 1991. Mapping the magnitude of sodicity in part of the Indo-Gangetic plains of Uttar Pradesh, northern India using Landsat-TM data. *International Journal of Remote Sensing* 12(3):419-425.

Rao, B.R.M. and L. Venkataratnam. 1991. Monitoring of salt affected soils: a case study using aerial photographs, Salyut-7 space photographs, and Landsat TM data. *Geocarto International* 6(1):5-11.

Saterwhite and Henley. 1987. Spectral characteristics of selected soils and vegetation in northern Nevada and their discrimination using band ratio techniques. *Remote Sensing of Environment* 23:155-175.

Sehgal, J.L. and P.K. Sharma. 1988. An inventory of degraded soils of Punjab (India) using remote sensing technique. *Soil Survey and Land Evaluation* 8(3):166-175.

Sharma, R.C. and G.P. Bhargava. 1988. Landsat imagery for mapping saline soils and wet lands in north-west India. *International Journal of Remote Sensing* 9(1):39-44.

Sujatha, G., R.S. Dwivedi, K. Sreenivas, and L. Venkataratnam. 2000. Mapping and monitoring of degraded lands in part of Jaunpur district of Uttar Pradesh using temporal spaceborne multispectral data. *International Journal of Remote Sensing* 21(3):519-531.

Verma, K.S., R.K. Saxena, A.K. Barthwal, and S.N. Deshmukh. 1994. Remote sensing technique for mapping salt-affected soils. *International Journal of Remote Sensing* 15(9):1901-1914.

APPENDIX

Signature separability (Transformed divergence values) for training signatures east of Blakely Canal.

	1	2	3	4	6
FCC432	Saline-sodic	Sodic	Slightly saline	Saline	Nonsaline
Saline-sodic (1)	0	2000	2000	2000	2000
Sodic (2)	2000	0	265	2000	1869
Slightly saline (3)	2000	265	0	2000	1617
Saline (4)	2000	2000	2000	0	2000
Nonsaline (6)	2000	1869	1617	2000	0

	1	2	3	4	6
FCC453	Saline-sodic	Sodic	Slightly saline	Saline	Nonsaline
Saline-sodic (1)	0	2000	2000	2000	2000
Sodic (2)	2000	0	1194	2000	1862
Slightly saline (3)	2000	1194	0	2000	1994
Saline (4)	2000	2000	2000	0	2000
Nonsaline (6)	2000	1862	1994	2000	0

	1	2	3	4	6
FCC457	Saline-sodic	Sodic	Slightly saline	Saline	Nonsaline
Saline-sodic (1)	0	2000	2000	2000	2000
Sodic (2)	2000	0	1402	2000	1984
Slightly saline (3)	2000	1402	0	2000	2000
Saline (4)	2000	2000	2000	0	2000
Nonsaline (6)	2000	1984	2000	2000	0

	1	2	3	4	6
TassCap	Saline-sodic	Sodic	Slightly saline	Saline	Nonsaline
Saline-sodic (1)	0	2000	2000	2000	2000
Sodic (2)	2000	0	1019	2000	1436
Slightly saline (3)	2000	1019	0	2000	1293
Saline (4)	2000	2000	2000	0	2000
Nonsaline (6)	2000	1436	1293	2000	0